Colloids and Surfaces A 604 (2020) 125326

Contents lists available at ScienceDirect

Colloids and Surfaces A

journal homepage: www.elsevier.com/locate/colsurfa

# A dissipative particle dynamics and discrete element method coupled model for particle interactions in sedimentation toward the fabrication of a functionally graded material

Chensen Lin[a,b], Lingqi Yang[b], Fangliang Chen[b], Shuo Chen[a], Huiming Yin[b,*]

[a] School of Aerospace Engineering and Applied Mechanics, Tongji University, Shanghai 200092, PR China
[b] Department of Civil Engineering and Engineering Mechanics, Columbia University, New York, New York 10027, USA

## GRAPHICAL ABSTRACT

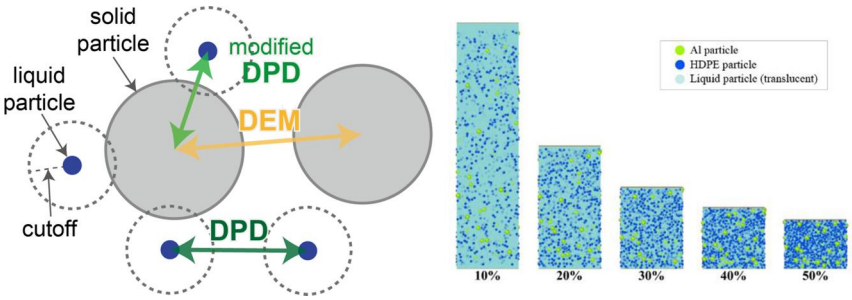


## ARTICLE INFO

*Keywords:*
Sedimentation
Particle simulation
Dissipative particle dynamics (DPD)
Discrete element method (DEM)
Functionally graded materials

## ABSTRACT

A new particle-based simulation model to tackle the problem of micrometer scale particle motion in sedimentation at low to high concentration is presented. In this model, the solid particle interactions are described by discrete element method (DEM), while the liquid part are simulated by a mesoscale fluid simulation method dissipative particle dynamics (DPD). The coupling part are modified DPD potential with tuned parameters to ensure the correct hydrodynamic interaction between solid and liquid particles. Experiments are further conducted to compare the simulation phenomenon. The well agreement verifies the presented coupling is an effective model for this scenario. Some new results for sedimentation of different initial conditions, such as liquid volume, and particle size are then presented. This new model can be a powerful tool to simulate micrometer particles sedimentation process, which is important in material design and quality control of sedimentation based FGM manufacture.

## 1. Introduction

Functionally graded materials (FGMs) are a type of heterogeneous materials that possess a position-dependent microstructure, resulting in continuous variation of material properties with position at the macroscale [1]. Usually, the volume fractions of the constituents in an FGM vary gradually, leading to a continuous variation of the effective thermal, electrical, or mechanical properties, which a homogenous material does not exhibit [2,3]. FGMs have attracted extensive attention from both academia and industry because of their unique material characteristics not offered by conventional materials. Recent research conducted at Columbia University [4,5] has shown its great potential in

* Corresponding author.
*E-mail address:* yin@civil.columbia.edu (H. Yin).

https://doi.org/10.1016/j.colsurfa.2020.125326
Received 22 April 2020; Received in revised form 19 July 2020; Accepted 20 July 2020
Available online 22 July 2020

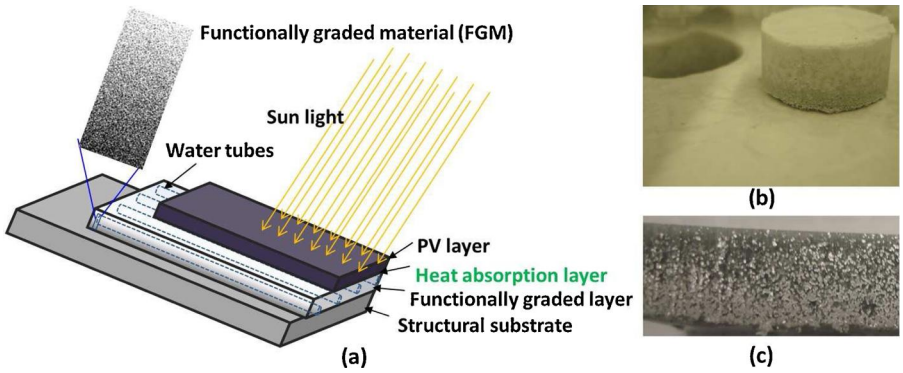


**Fig. 1.** Sedimentation-based manufacturing of an FGM for a multifunctional solar roofing panel: (a) Schematic illustration of the BIPVT roofing pane; (b) a graded mix of Al and HDPE particles produced by sedimentations; and (c) the FGM obtained by sintering the graded mix.

harvesting solar energy efficiently by using an FGM in a building integrated photovoltaic thermal (BIPVT) roofing panel. Fig.1 schematically illustrates the innovative idea of this BIPVT in that a photovoltaic (PV) solar cell laminated by a protective layer directly transfers solar energy into electricity; the PV layer bonds to a structural substrate through an FGM layer, in which water tubes are cast to harvest heat energy by water flow and thus control the panel temperature. The two components of this FGM layer are aluminum (Al) and high-density polyethylene (HDPE). The co-sedimentation method has been used toward producing FGM from powders [6].

Particle sedimentation has been attracting considerable research efforts. Different numerical methods have been developed based on the level of length scale. In cases dealing with colloidal particles, polymer molecules and fibers, where length scale is small, the dynamics of suspensions are governed by short range interparticle forces such as van der Waals, Brownian motion due to thermal fluctuations, and shor and long range hydrodynamic interactions transmitted by the suspending fluid. The Reynolds number is usually very small and the motion of the fluid is governed by Stokes equation. Some methods are devised for this type of suspension flow, such as Stokesian Dynamics Method [7] and Force Couplling Method [8]. In cases dealing with sand grains and gravel, the length scale is large, dynamics of such flows are dominated by particle-particle collisions, and the surrounding fluid is expected to play a very subdued role in the phenomenon. Due to the discontinuous granular nature, there is no comprehensive understanding of such material and the derivation of a continuous constitutive equation is not straight-forward. A promising method to tackle granular flows is DEM, introduced by Cundall and Strack in 1979 [9]. It is a particle-based method simplified from the contact mechanics theory [9]. It has been widely used in particulate flows [10].

The intermediate level of length scale between Stokes regime and granular matter is probably the most challenging length scale: moderately to highly concentrated suspensions of nearly macroscale particles in a fluid. It is also the scale of the sedimentation process for FGM. In such flows, the particulate Re is indeed not small and the hydrodynamic forces need to be considered. Consequently, a proper model of collisions is required for two main reasons: the probability of collisions is sufficiently high and lubrication forces are not large enough anymore to prevent particles from touching each other. The simulation of this type of flow is a non-trivial task due to the constantly evolving space occupied by the fluid as particles move. The first class of numerical model, the boundary fitted approach, is very complex because of remeshing requirement of the fluid domain and corresponding projection of flow fields on the updated mesh at every time step [11]. The second class, the non-boundary fitted method, is usually easier to implement (the grid is fixed) and more efficient for the simulation of a large number of particles. This class includes Lattice-Boltzmann Method (LBM), Immersed Boundary Method (IBM). In most of literature contributions in this class, the collision model is a simple repulsive force that prevents the overlap of two particles. As the volume fraction increases, the rise of collisions probability requires the use of a more proper collision model that is crucial to the study of particulate flows, especially at high Re. The third class is coupling DEM method with a computational fluid dynamics solver. Various coupled model have been studied, including: Cleary and Prakash [12] couple DEM with a SPH approach, Komiwes et al. [13] couple DEM with an IBM, Singh et al. [14] couple DEM with a DLM/FD method. The coupled framework improves the flexibility and accuracy of the model and has attracted considerable research attempts.

In this work, we proposed a new coupled Dissipative Particle Dynamics-Discrete Element Method (DPD-DEM) method, aiming the problem of moderate to high concentration of micrometer solid particles setting in liquid. The new model has three main advantages: (1) DEM ensures the solid particle collision cased by high concentration been properly modeled; (2) In length scale of micrometer, the abovementioned N–S equation solver did not include the thermal fluctuation. DPD is a thriving fluid simulation method for mesoscale phenomenon. It naturally involves the thermal fluctuations as well as short and long range hydrodynamic interactions. It has been applied to many mesoscale fluid problems, such as polymer solutions [15,16], red blood cells [17,18], and droplet motion [19,20]. (3) The particle nature of both DPD and DEM makes the coupled framework straightforward and reduces the computational cost. This avoids problems raised by coupling a particle-based and a grid-based method.

The remainder of the paper is organized as follows: Section 2 presents the overview of the algorithm; Section 3 contains benchmark validation with experiments; Section 4 focuses on some new results for sedimentation of different initial conditions, such as liquid volume, and particle size; Section 5 summarizes this work with some conclusive remarks.

## 2. Simulation technique: coupled DPD-DEM

### 2.1. Dissipative particle dynamics

Hoogerbrugge and Koelman [21] initially proposed DPD in 1992, Español and Warren [22] then modified it to recover the Gibbs distribution as the stationary solution to the Fokker-Plank equation. This method clusters a certain amount of molecules into a single particle in which the coarse-graining parameter gives the number of molecules per DPD particle [23]. Instead of defining potential energy directly as classic MD potential, Español et al. [23] used three inter-particle forces that lie along their center-to-center line, thus conserving linear momentum. $\mathbf{F}_{ij} = \mathbf{F}_{ij}^{C} + \mathbf{F}_{ij}^{D} + \mathbf{F}_{ij}^{R}$, where $F_{ij}^{C}$ represents a purely repulsive conservative force, $F_{ij}^{D}$ a dissipative or frictional force to consider the effects of viscosity that slows down the particles with respect to each other, and $F_{ij}^{R}$ a random force to take into account the thermal or vibrational energy of the system. All three forces are calculated within a cutoff radius $r_c$, beyond which the forces are considered negligible.

$$\mathbf{F}_{ij}^{\mathrm{C}} = w^{\mathrm{C}}(r_{ij})\boldsymbol{e}_{ij} \tag{1}$$

$$\mathbf{F}_{ij}^{\mathrm{D}} = -\gamma w^{\mathrm{D}}(r_{ij})[v_{ij}\cdot e_{ij}]\boldsymbol{e}_{ij} \tag{2}$$

$$\mathbf{F}_{ij}^{\mathrm{R}} = \sigma w^{\mathrm{R}}(r_{ij})\theta_{ij}\boldsymbol{e}_{ij} \tag{3}$$

where $r_{ij} = |\boldsymbol{r}_{ij}| = |\boldsymbol{r}_i - \boldsymbol{r}_j|$ represents the distance between two particles $i$ and $j$, $\boldsymbol{e}_{ij} = \boldsymbol{r}_{ij}/r_{ij}$ is the unit vector from particles $j$ to $i$, $\theta_{ij}$ is a Gaussian white noise function with symmetry property $\theta_{ij} = \theta_{ji}$ to ensure the total conservation of momentum and consider the stochastic properties which will be elaborated later. $\gamma$ and $\sigma$ are the coefficients of the dissipative and random forces, respectively, which satisfy the Gibbsian equilibrium:

$$w^{\mathrm{D}}(r) = [w^{\mathrm{R}}(r)]^2 \tag{4}$$

$$\sigma^2 = 2\gamma k_{\mathrm{B}}T/m \tag{5}$$

where $k_{\mathrm{B}}$ is the Boltzmann constant and $T$ is the equilibrium temperature. Since the algorithm involves the relative velocities and interactions between particles, the isotropic Galilean invariant thermostat can preserve hydrodynamics. A simple decaying function of distance can define the conservative force weight function and is represented by:

$$w^{\mathrm{C}}(r_{ij}) = \begin{cases} a_{ij}\left(1 - \dfrac{r_{ij}}{r_{\mathrm{c}}}\right) & r_{ij} \le r_c \\ 0 & r_{ij} > r_c \end{cases} \tag{6}$$

The dissipative and random weight functions take the general form:

$$w^{\mathrm{D}}(r_{ij}) = [w^{\mathrm{R}}(r_{ij})]^2 = \begin{cases} \left(1 - \dfrac{r_{ij}}{r_{\mathrm{c}}}\right)^2 & r_{ij} \le r_c \\ 0 & r_{ij} > r_c \end{cases} \tag{7}$$

Groot and Warren (1997) thoroughly reviewed the DPD method and established several useful guidelines for choosing DPD force parameters. By matching the dimensionless compressibility of water at room temperature, an analytical form was derived for the repulsive force parameter of water-water particles

$$a = \frac{75k_BT}{\rho_{\mathrm{DPD}}} \tag{8}$$

where $\rho_{\mathrm{DPD}}$ is the number density in simulation. Currently, most studies in literature apply this parameter established for water. However, in fabricating the FGM shown in Fig. 1, it is necessary to replace water with ethanol to avoid corrosion of aluminum particles. Thus, the force parameters need to be modified for ethanol in DPD simulation. By following Groot and Warren [24], one can obtain the relation between $a$ and dimensionless compressibility $\kappa$:

$$\kappa^{-1} = 1 + \frac{2\alpha a\rho_{\mathrm{DPD}}}{k_{\mathrm{B}}T} \approx 1 + \frac{0.2a\rho_{\mathrm{DPD}}}{k_{\mathrm{B}}T} \tag{9}$$

Using $\kappa_{\mathrm{ethanol}}^{-1} \approx 20$, the coefficient of conservative force between ethanol-ethanol particles is expressed as:

$$a_{\mathrm{e-e}} = \frac{95k_{\mathrm{B}}T}{n_{\mathrm{DPD}}} \tag{10}$$

### 2.2. Discrete element method

Unlike DPD, in which a particle is represented by a mathematical point, a particle in DEM has a radius. Conventional DEM rotates the particle by adding the expression of torque into the governing equations:

$$\frac{d\boldsymbol{r}}{dt} = \boldsymbol{V},\ m\frac{d\boldsymbol{V}}{dt} = \boldsymbol{F},\ I\frac{d\omega}{dt} = \boldsymbol{T}_r \tag{11}$$

where $\boldsymbol{r}$, $\boldsymbol{V}$, $I$, $\omega$ and $\boldsymbol{T}_r$ represent the position, velocity, momentum of inertia, rotation speed, and torque.

In this study, since the DEM particle can be considered as a rigid body compared with the soft DPD particles, the linear spring-dashpot (LSD) model is applied to describe the contact in a linear regime with simplicity. In LSD, a normal spring and dashpot, a tangential spring and dashpot, and torque [9] express the interaction between two particles. It has been simplified by only considering the spring force as an imposing force based on the relative velocity between particles to simulate the dashpot force [25]. The normal ($\boldsymbol{F}_{\mathrm{n}}^{ij}$) and tangential forces ($\boldsymbol{F}_{\mathrm{t}}^{ij}$) can be decomposed to the spring and dashpot (dissipative force) respectively. The formulation of the force potential is summarized below:

$$\boldsymbol{F}_{\mathrm{n}}^{ij} = k_{\mathrm{n}}\Delta r_{\mathrm{n}}^{ij}\boldsymbol{n}^{ij} - C_{\mathrm{n}}\boldsymbol{V}_{\mathrm{n}}^{ij} \tag{12}$$

$$\boldsymbol{F}_{\mathrm{t}}^{ij} = \begin{cases} -k_{\mathrm{t}}\Delta r_{\mathrm{t}}^{ij}\boldsymbol{t}^{ij} - C_{\mathrm{t}}\boldsymbol{V}_{\mathrm{t}}^{ij} & if\ |\boldsymbol{F}_{\mathrm{t}}^{ij}| \le \mu|\boldsymbol{F}_{\mathrm{n}}^{ij}| \\ -\mu\,|F_{\mathrm{n}}^{ij}|\,\boldsymbol{t}^{ij} & if\ |\boldsymbol{F}_{\mathrm{t}}^{ij}| > \mu|\boldsymbol{F}_{\mathrm{n}}^{ij}| \end{cases} \tag{13}$$

$$\boldsymbol{T}_{\mathrm{r}}^{ij} = -L^i\boldsymbol{n}^{ij} \times \boldsymbol{F}_{\mathrm{t}}^{ij} \tag{14}$$

where $\Delta r_{\mathrm{n}}^{ij} = |\Delta\boldsymbol{r}_{\mathrm{n}}^{ij}|$ and $\Delta r_{\mathrm{t}}^{ij} = |\Delta\boldsymbol{r}_{\mathrm{t}}^{ij}|$are the normal and tangential displacements respectively, $\boldsymbol{n}^{ij}$ and $\boldsymbol{t}^{ij}$ are the normal and tangential direction, $\boldsymbol{V}_{\mathrm{n}}^{ij}$ and $\boldsymbol{V}_{\mathrm{t}}^{ij}$ are the normal and tangential relative velocity, $L^i = |\boldsymbol{L}^i|$, and $\boldsymbol{L}^i$ stands for the vector from the center of particle $i$ to the contact point. $k_{\mathrm{n}}$, $C_{\mathrm{n}}$, and $k_{\mathrm{t}}$, $C_{\mathrm{t}}$ are the spring stiffness and dashpot damping coefficient along the normal and tangential directions respectively. $\mu$ is the friction coefficient.

The normal damping coefficient can be derived analytically as [26]

$$C_{\mathrm{n}} = 2\sqrt{m_{\mathrm{eff}}k_{\mathrm{n}}}\frac{\ln e_{\mathrm{n}}}{\sqrt{\ln^2 e_{\mathrm{n}} + \pi^2}} \tag{15}$$

where $m_{\mathrm{eff}} = m^I m^J/(m^I + m^J)$ is the effective mass. $e_{\mathrm{n}}$ (normal restitution coefficient) for aluminum and HDPE particles can be found in [27,28]. The tangential spring stiffness and damping coefficients are set as [29]

$$k_{\mathrm{t}} = \frac{2}{7}k_{\mathrm{n}} \tag{16}$$

$$C_{\mathrm{t}} = \frac{1}{2}C_{\mathrm{n}} \tag{17}$$

The critical time step, or the collision duration, is derived as [26]

$$t_{\mathrm{c,n}} = \pi\left(\frac{k_{\mathrm{n}}}{m_{\mathrm{eff}}} - \frac{C_{\mathrm{n}}^2}{4m_{\mathrm{eff}}^2}\right) \tag{18}$$

Following the convention, the time step is chosen below $\Delta t = \min\left(\frac{t_{\mathrm{c,n}}}{50}\right)$ to maintain a stable simulation.

### 2.3. Algorithm and implementation of the coupled model

#### 2.3.1. DPD-DEM coupling

To model solid particle, Chen et al. [30] proposed a rough sphere model that uses numerous particles. This method can form solid particles of different shape. Yang and Yin [31] proposed using a single particle to represent a solid particle, introducing a core radii and altering the interaction parameters between its surrounding liquid particle, see Fig.2. By this way, the liquid DPD fluid particle cannot enter the force cut-off range, which produces a similar effect as in the rough sphere model. The difference is that the particles in the reduced rough sphere model are smooth, spherical, and structureless. Although the rough sphere model has certain advantages, its high computational cost limits its applications. Considering the solid particles are almost spherical as illustrated in Section 3 and the huge number, the reduced rough sphere model is used in this study.

Fig. 3 illustrates the main concept of our model. The collision between solid particles are modeled by DEM, while the interaction between liquid-liquid particles are modeled by DPD. The liquid-solid interaction is using a modified DPD model.

The modified DPD model for liquid-solid interaction is proposed by

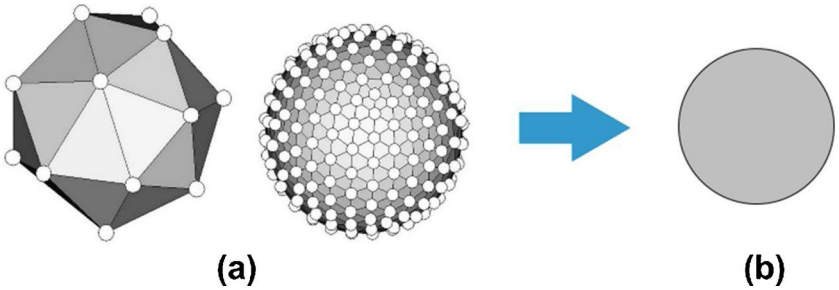


**Fig. 2.** Solid particle model: (a) Rough sphere model [30]; (b) Reduced rough sphere model [31].

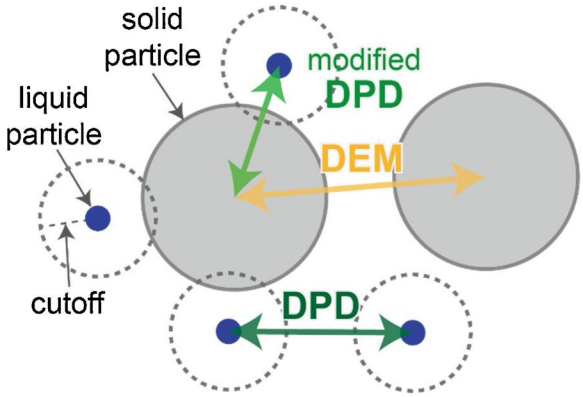


**Fig. 3.** Illustration of DPD/DEM coupled model.

Yang and Yin [31]. They provided a systematic study in selecting the parameters for different conditions through matching the Stokes' law. An analytical expression of the minimum $a_{\mathrm{Al-liquid}}$ as a function of the $\rho_{\mathrm{DPD}}$ is provided as follows:

$$a^{\min}_{\mathrm{Al-liquid}} = 10^{-(0.0222\rho_{\mathrm{DPD}}+0.255)\ln[0.03/(1178.460)\rho_{\mathrm{DPD}}^{-1.450}]} \tag{19}$$

They also concluded two empirical equations of Eqs. (20) and (21) to help choose $r^{\mathrm{cut}}_{\mathrm{Al}}$ and $a^{\min}_{\mathrm{Al-liquid}}$ in terms of $r_{\mathrm{Al}}$.

$$r^{\mathrm{cut}}_{\mathrm{Al}} = 1.249r_{\mathrm{Al}} + 0.369 \tag{20}$$

$$a^{\min}_{\mathrm{Al-liquid}} = 10^{-(0.281r_{\mathrm{Al}}+0.202)\ln[0.03/(28.192(r_{\mathrm{Al}})-2.242)]} \tag{21}$$

### 2.3.2. Coarse-graining level of liquid particle

DPD is different from MD since it represents a cluster of molecules instead of a single atom, thus making DPD a coarse-grained method. The tunable coarse-graining level in DPD needs to be determined for specific cases. For the sedimentation case, the coarse-graining level should be selected very carefully because liquid DPD particle should be small enough to provide continuum force on solid particles. In this subsection, the influence of the coarse-graining level on the sedimentation process will be investigated. Since the diameter of solid particle is determined, we use diameter ratio ($n_{\mathrm{ratio}}$) between solid and liquid particles to mark the liquid particle size.

Two group cases are presented in this subsection. Table 1 shows a summary of the simulation parameter inputs. Notice that suspension height and gravity ($g_{\mathrm{DPD}}$) should change according to coarse-graining level.

In the first group, the size ratio between solid and liquid is set as $n_{\mathrm{ratio}} = 1$ to minimize the computational cost. The volume fraction of Al particles varies from 5% to 20 %. Numerical tests reveal a non-physical meaningful behavior that the settling of Al particles moves up and down. Fig. 4(a) provides the temperatures of the liquid particles, centroids, and average settling velocities of Al particles along the gravitational direction. The temperature profile exhibits big fluctuation in the beginning and reveal the mean temperature can't reach reference temperature (1.0) except the 5% case. To numerically analyze this phenomenon, Fig. 4(b) plot the centroids and average settling velocities evolution over time. As $\phi^{\mathrm{Al}}$ increases, the settling seems not happing, while solid particles fluctuate up and down together.

**Table 1**
Simulation inputs for the sedimentation with different $\phi_{\mathrm{solid}}$ and $n_{\mathrm{ratio}}$ (DPD units).

| | Group 1 | Group 2 |
|---|---|---|
| $\phi_{\mathrm{solid}}$ | 5%/10%/15%/20% | 5% |
| $n_{\mathrm{ratio}}$ | 1 | 1/2/3/4/5 |
| $g_{\mathrm{DPD}}$ | 0.202 | 0.202/0.0252/0.00748/0.00315/0.00162 |
| suspension height | 200 | 200/400/600/800/1000 |

The up and down motion suggests two fundamental issues: (1) DPD liquid cannot provide sufficient and consistent viscous force; (2) particles cannot move freely. This phenomenon is principally related to the coarse-graining level up limit for the liquid particle. Fig. 5 shows a simple but vivid demonstration of the liquid coarse-graining effect, noticing that in our proposed reduced rough sphere model, the strong interaction between solid-liquid particles prevents the fluid particles from penetrating the solid particle. If the average space among solid particles is narrow, the lower fluid particles will be pushed downward while the upper fluid particles loses contact with solid particles. After a certain time, the extremely inconsistent local density of liquid particles will push the solid particles upwards.

In order to investigate the size ratios effect, $n_{\mathrm{ratio}}$ is increased from 1 to 5. As a result, the suspension height in the DPD units becomes larger. Hence, the centroid of Al particles with different $n_{\mathrm{ratio}}$ shown in Fig. 6 is normalized. When $n_{\mathrm{ratio}} \geq 3$, the temperature profile is relatively stable, and the noise is much smaller compared with that of when $n_{\mathrm{ratio}} = 1$ or 2. The average settling velocity profile in Fig. 6(b) also reflects the same trend. When $n_{\mathrm{ratio}} = 4,5$, we can almost ignore such a fluctuation. The centroid plot shown in Fig. 6(b) can also confirm this fact. The curve is almost smooth when $n_{\mathrm{ratio}} = 4$ or 5 while saw shape bumps appear when $n_{\mathrm{ratio}} \leq 3$. To prevent the problem discussed above, the parameter $n_{\mathrm{ratio}}$ should be greater than 4 in the DPD/DEM coupling model.

### 2.3.3. Simulation of particle sedimentation

With the established guidelines, the coupled DPD-DEM model is then used to simulate two different types of particles, Aluminum and HDPE, settling down in liquid ethanol. The periodic boundary condition is applied along the $x$ and $y$ directions to eliminate the influence of the side wall. Fig. 7 illustrates the simulation domain.

The diameter of the particle is a crucial factor for sedimentation. In experiment, the size of the particle usually follows a Gaussian distribution. However, in previous literature, solid particles are set to monosize to simplify the model. In this study, we set the solid particle

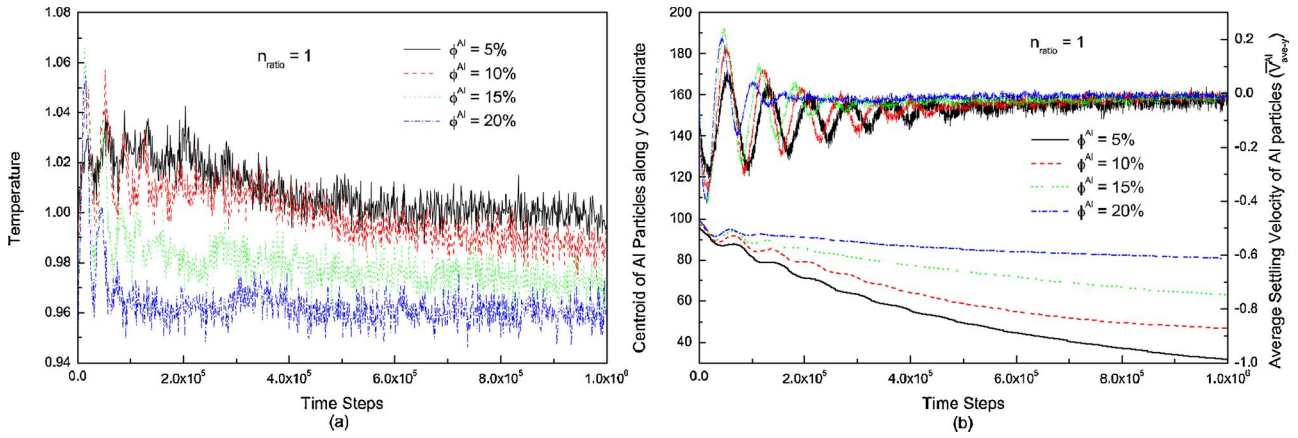


**Fig. 4.** Comparison of (a) DPD fluid temperature T, (b) centroid and average settling velocity $V_{ave}^{Al}$ of Al particles along the gravitational direction with different volume fractions.$\varnothing^{Al}$

size with Gaussian distribution like experiment, helping to better catch the detailed structure while unavoidably bringing some computational overhead.

The simulation procedure has 3 stages like the experiments. The first stage is preparing the well-mixed suspension. The Al, HDPE, and liquid particles are first randomly generated to fill the domain. The system is then carefully relaxed to push apart the particles overlapped. The second stage is sedimentation, the most time-consuming part. The last stage corresponds to the dry treatment in the experiment in which the liquid is removed and all the solid particles eventually packed as an FGM mix.

## 3. Experiment validation

A series of experimental tests were conducted to validate the simulation results predicted by our model. The solid particles are a mixture of spherical Al particles and HDPE powders. This test used the H-30 spherical aluminum particles provided by Reade Advanced Materials which exhibit a wide size distribution ranging from 15μm to 58μm. No.270 and No.325 ASTM sieves sieved the original Al particles to reach a narrower size distribution of 38 μm to 45 μm. Fig. 8 shows the size distribution which is measured by Mastersizer 2000 Particle Analyzer. The high-resolution cold field emission scanning electron microscope (SEM) examined the shapes of particles. Al and HDPE particles are both fairly spherical as shown in Fig. 9.

The volume fraction of solid is 10 % and volume ratio of Al/HDPE is set to be 1:3. After pouring the solid particles into the liquid, considerable air bubbles are observed in the suspension, which will affect the gradation. To eliminate such effects, the suspensions were degassed in the vacuum by gradually decreasing the air pressure down to 45 T. Then the suspension is put still for sedimentation. Fig. 10 illustrates the evolution of the sedimentation process. The sediments were maintained for 24 h until the supernatant became quite clear.

Then, the sediments were fully dried and divided into five segments with equal height. The density of sediments was measured by a modified Rice method developed by the authors [32]. Based on the test density of the dried mixture, the volume fraction of Al ($\phi^{Al}$) and HDPE ($\phi^{Al}$) in each layer can be determined by

$$\phi^{Al} = \frac{\rho^{Al} - \rho^{M}}{\rho^{Al} - \rho^{HDPE}},\ \phi^{HDPE} = \frac{\rho^{M} - \rho^{HDPE}}{\rho^{Al} - \rho^{HDPE}} \tag{22}$$

where $\rho^{Al}$, $\rho^{HDPE}$, and $\rho^{M}$ are the density of Aluminum, HDPE, and dried mixtures respectively.

Table 2 gives the summary of the experiment and the simulation details, $D$ indicates the diameter of the solid particle.

Fig. 11 shows the comparison of the gradation between experiment and simulation results. It shows that the numerical simulation generally agrees well with the experiment. Overall, more aluminum particles are settled in the bottom layer while HDPE particles are in the top layer, indicating a successfully formed gradation.

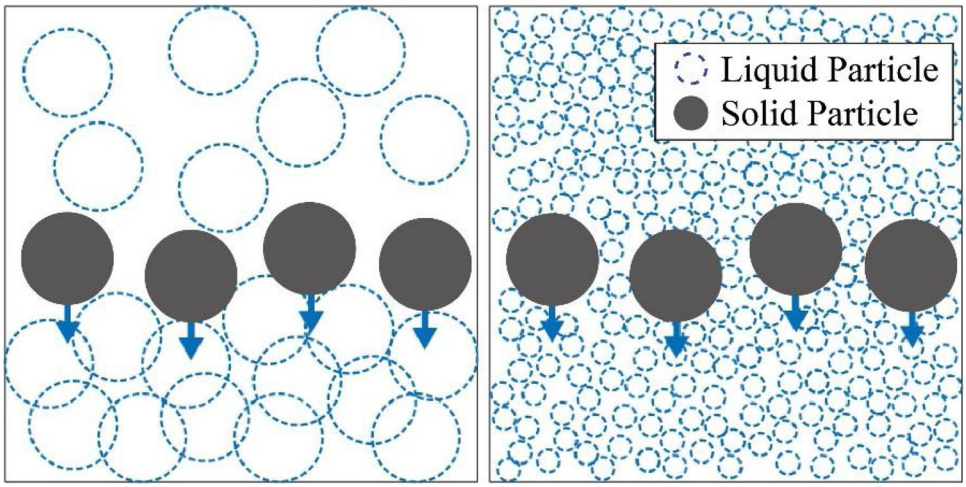


**Fig. 5.** Schematic demonstration of the size ratio effect.

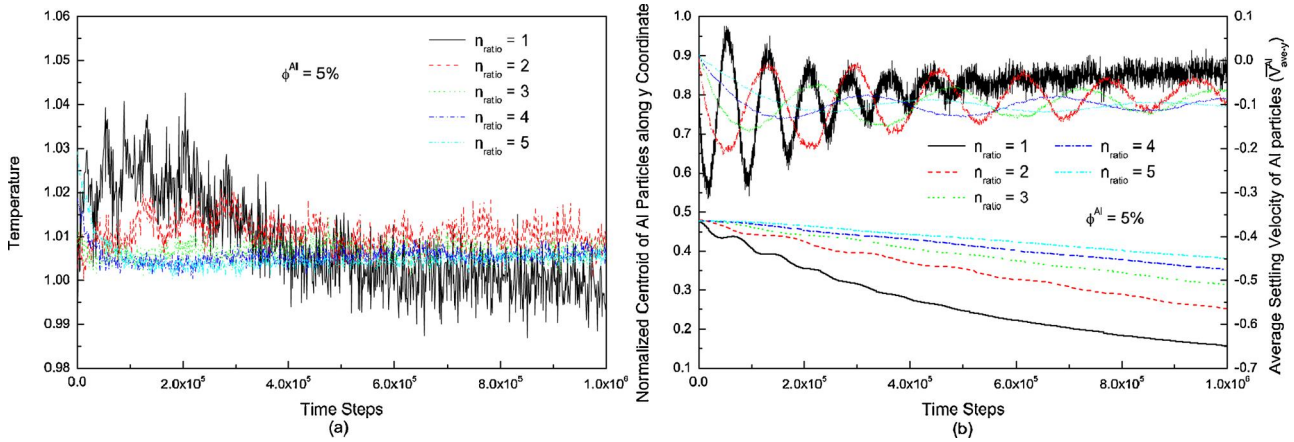


**Fig. 6.** Comparison of (a) DPD fluid temperature T (b) centroid and average settling velocity $V_{ave}^{Al}$ of Al particles along gravitational direction with different size ratios.$n_{ratio}$

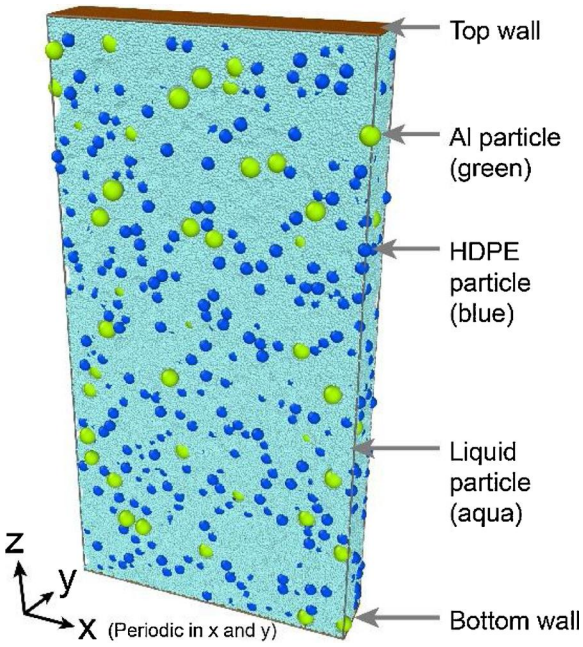


**Fig. 7.** Illustration of computational domain.

## 4. Parametrical studies

### 4.1. Liquid volume

Many factors could influence the sediment gradation, the liquid volume is one of them. In this subsection, we use solid concentration ($\phi_{solid}$) to characterize the liquid volume used in the sedimentation. Five cases with different $\phi_{solid}$, namely 10 %, 20 %, 30 %, 40 %, 50 %, are compared. Fig. 12 illustrates the initial configurations of all cases. It is worth noting that the greatest fraction of space occupied by spheres is around 74 %, implying $\phi_{solid}$ = 50% a relative high concentration.

The different gradation of sediment in the five cases were plotted in Fig. 13. It shows that the higher solid concentration ($\phi_{solid} \geq 30$ %) leads to poor gradations. This is because crowded solid particles in liquid has not enough room to move around, prevent the difference of setting velocity to take effect. We can learn that solid particle concentration higher than 30 % is not suitable for producing FGM. The $\phi_{solid}$= 20 % and 10 % cases share a similar Al-free top layer, while the general gradation curve is quite different. Researchers could customize a specific gradation through manipulating the liquid volume in sedimentation process.

### 4.2. Particle size

The mechanism behind the co-sedimentation method lies in the particles' different settling velocities. The basic relationship between

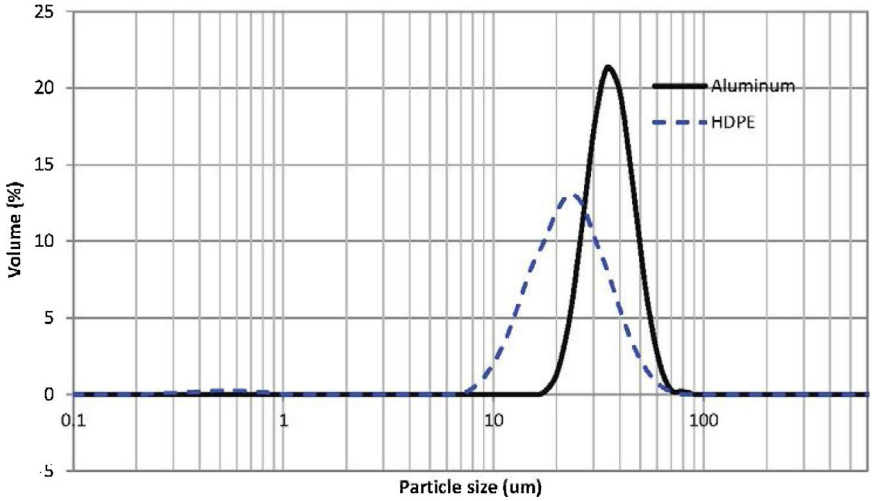


**Fig. 8.** Size distributions of the Al particle and the HDPE powder.

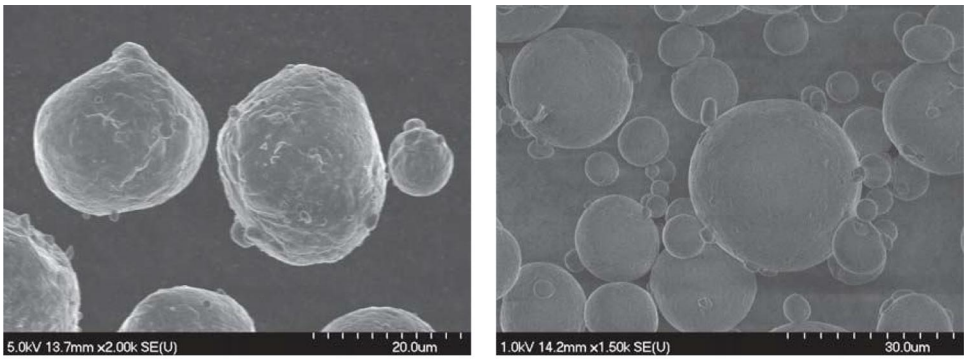


**Fig. 9.** SEM observations of particle shapes (a) aluminum and (b) HDPE.

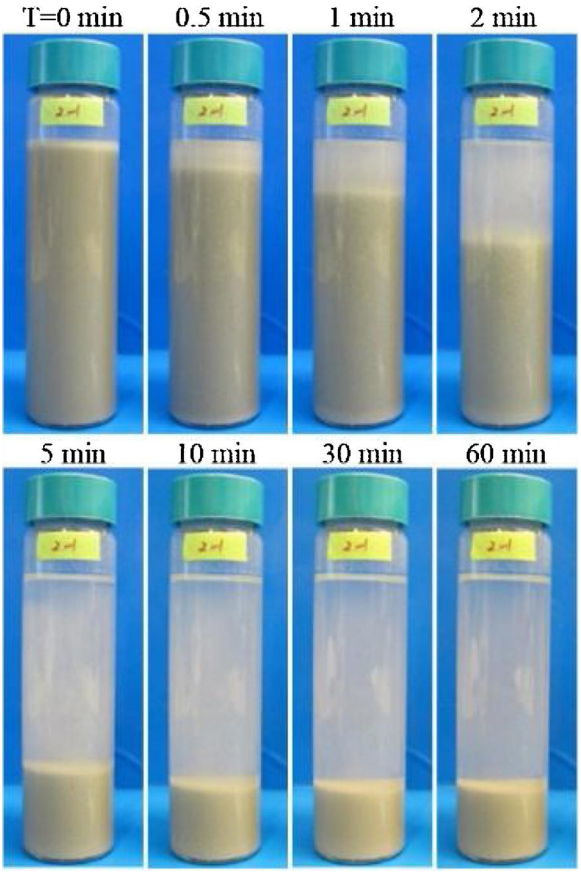


**Fig. 10.** Sedimentation process in glass vials.

**Table 2**
Summary of the experiment and simulation details.

| | Experiment | Simulation |
|---|---|---|
| Suspension Height | 82.79 mm | 300 (DPD units) |
| $D^{Al}$ | 38 – 45 μm | 7 – 9 (DPD units) |
| $D^{HDPE}$ | 21 – 28 μm | 4 – 6 (DPD units) |
| $\phi^{Al}$ | 2.5 % | 2.5 % |
| $\phi^{HDPE}$ | 7.5 % | 7.5 % |

the terminal velocity and the particle density and diameter is revealed in Stocks' law. By adjusting the particle size, one could control the difference of two type particles' terminal velocity, which determine the final sediments. To quantitatively investigate the effect of the particle

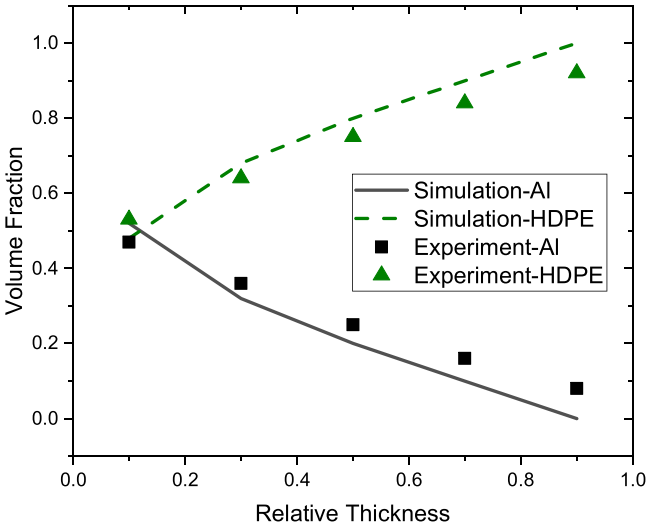


**Fig. 11.** Gradation comparison of the sedimentation composite between the experiment and the simulation.

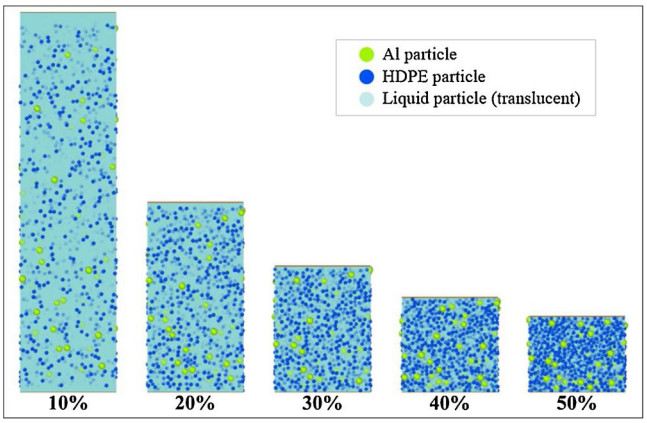


**Fig. 12.** Initial configuration of the mix at different solid volume fractions.

size, four different sizes of Al particles are studied, they are 28μm, 36μm, 42μm, and 50μm. The diameter of HDPE stays the same (24μm) in all cases. Fig. 14 shows the particle number in different cases. To maintain the solid volume fraction unchanged ($\phi_{Al}$ = 5% and $\phi_{HDPE}$ = 15%), the increase in Al particle size leads to decrease in particle numbers.

Fig. 15 presents the effect of Al diameter on the sediments. It generally shows that the gradation gets more obvious as the diameter of the

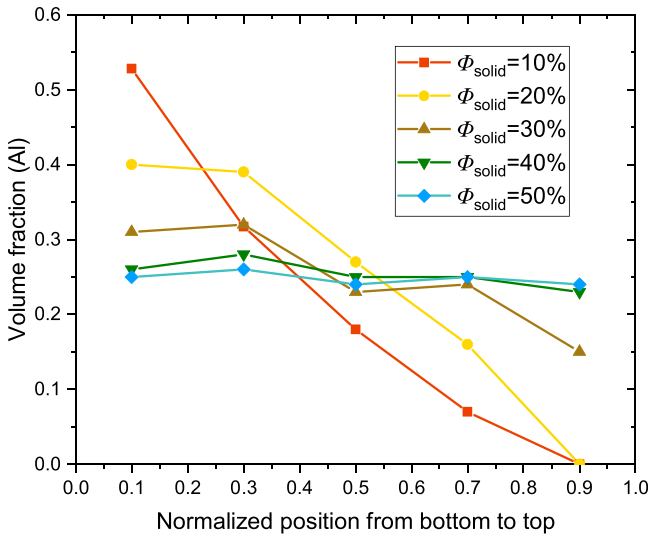


**Fig. 13.** The volume fraction variation in the thickness direction for the mix at different solid loads.

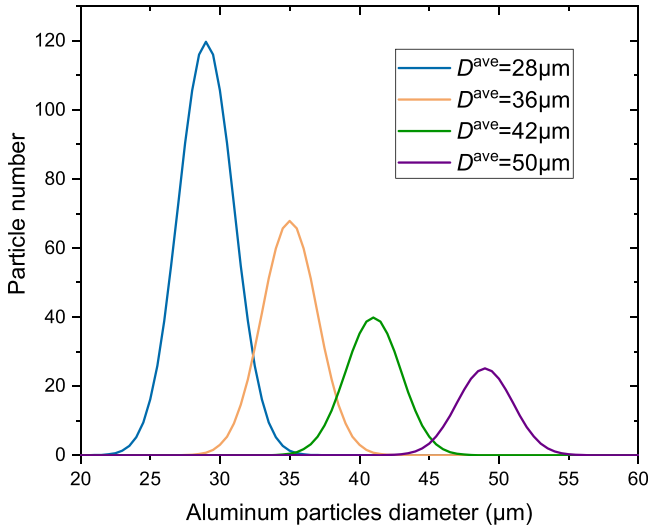


**Fig. 14.** Distribution of the aluminum particle diameter in different groups.

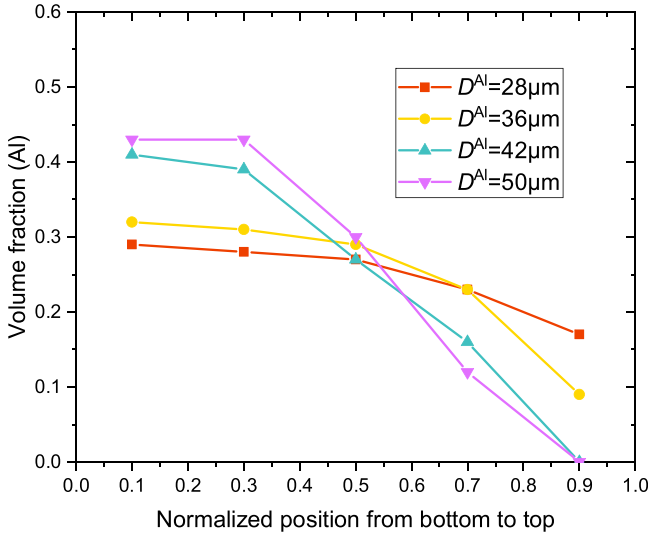


**Fig. 15.** The variation of volume fraction of the sediments with different Al particle sizes.

Al particles increases. The group with small Al size ($D_{Al}$ = 28μm) resulted a quite flat gradation and left a relatively high volume fraction of Al particles in the top layer. As $D_{Al}$ increases, Al began to vanish from the top layer, reaching 0% in both cases of $D_{Al}$ = 42μm and $D_{Al}$ = 50μm, which is ideal for our application. On the bottom side, it is interesting to notice that the two adjacent layers have very close volume fraction. This phenomenon could be resulted from the limited settling time for the bottom particles, which alleviates the separating of particles and makes the bottom sediment fraction significantly pinned to its initial composition fraction. Once the settling begins, both Al and HDPE particles reach the bottom and formed a relatively stable mixture because of the insufficient settling time. The simulation results disclosed in Fig. 15 could help to tailor a specific gradation curve by mixing Al particles with different sizes.

## 5. Conclusions

For the problem of micrometer scale solid particles sedimentation towards FGM fabrication, from low to very high concentration, a new coupled DPD-DEM numerical simulation model is proposed. The new model can handle both the solid particle collision, the mesoscale behavior of fluid, and has a straightforward coupling framework. To validate the new model, experimental studies were conducted and the results showed good agreement. Further studies reveal how various initial condition influence the final material gradation with the following conclusive remarks: (1) With the same solid particles, the more dilute the suspension, the finer the gradation; no considerable gradation was observed for a solid volume fraction higher than 40 %. (2) For a given particle size of HDPE, the gradation of the sediments gets more obvious as the size of the Al particles increases.

## CRediT authorship contribution statement

**Chensen Lin:** Conceptualization, Investigation, Software, Writing - original draft. **Lingqi Yang:** Conceptualization, Methodology, Software. **Fangliang Chen:** Writing - review & editing, Supervision. **Shuo Chen:** Writing - review & editing, Supervision. **Huiming Yin:** Resources, Supervision, Writing - review & editing, Project administration.

## Declaration of Competing Interest

The authors declare that they have no known competing financial interests or personal relationships that could have appeared to influence the work reported in this paper.

## Acknowledgments

This work is sponsored by the National Science Foundation CMMI 1762891, IIP 1738802, CMMI 0954717, and Air Force AF14-AT22, whose support is gratefully acknowledged. The first author would like to acknowledge the financial support from China Scholarship Council (CSC) (201506260045) for his one-year visit to Columbia University where this collaborative work was carried out. This work used the Extreme Science and Engineering Discovery Environment (XSEDE), which is supported by National Science Foundation grant number ACI-1053575.

## References

[1] Y. Miyamoto, W.A. Kaysser, B.H. Rabin, A. Kawasaki, R.G. Ford, Functionally graded materials: design, processing and applications, Springer Sci. Business Media (2013).
[2] H.M. Yin, L.Z. Sun, G.H. Paulino, Micromechanics-based elastic model for functionally graded materials with particle interactions, Acta Mater. 52 (2004) 3535–3543.
[3] A. Ray, S.V.G. Menon, Hydrodynamic simulation and thermodynamic

characterization of functionally graded material induced isentropic compression: towards optimum density profile, J. Appl. Phys. 110 (2011) 024905.
[4] H.M. Yin, D.J. Yang, G. Kelly, J. Garant, Design and performance of a novel building integrated PV/thermal system for energy efficiency of buildings, Sol. Energy 87 (2013) 184–195.
[5] D. Yang, H. Yin, Energy conversion efficiency of a novel hybrid solar system for photovoltaic, thermoelectric, and heat utilization, IEEE Trans. Energy Convers. 26 (2011) 662–670.
[6] F.L. Chen, X. He, H.M. Yin, Manufacture and multi-physical characterization of aluminum/high-density polyethylene functionally graded materials for green energy building envelope applications, Energy Build. 116 (2016) 307–317.
[7] A. Sierou, J.F. Brady, Accelerated stokesian dynamics simulations, J. Fluid Mech. 448 (2001) 115–146.
[8] E. Climent, M.R. Maxey, Numerical simulations of random suspensions at finite Reynolds numbers, Int. J. Multiph. Flow. 29 (2003) 579–601.
[9] P.A. Cundall, O.D. Strack, A discrete numerical model for granular assemblies, Geotechnique 29 (1979) 47–65.
[10] Y. Guo, J.S. Curtis, Discrete element method simulations for complex granular flows, Annu. Rev. Fluid Mech. 47 (2015) 21–46.
[11] A. Wachs, A DEM-DLM/FD method for direct numerical simulation of particulate flows: sedimentation of polygonal isometric particles in a Newtonian fluid with collisions, Comput. Fluids 38 (2009) 1608–1628.
[12] P.W. Cleary, M. Prakash, Discrete-element modelling and smoothed particle hydrodynamics: potential in the environmental sciences, Philos. Transact. A Math. Phys. Eng. Sci. 362 (2004) 2003–2030.
[13] V. Komiwes, P. Mege, Y. Meimon, H. Herrmann, Simulation of granular flow in a fluid applied to sedimentation, Granul. Matter 8 (2006) 41–54.
[14] P. Singh, T.I. Hesla, D.D. Joseph, Distributed Lagrange multiplier method for particulate flows with collisions, Int. J. Multiph. Flow. 29 (2003) 495–509.
[15] S. Pal, C. Seidel, Dissipative particle dynamics simulations of polymer brushes: comparison with molecular dynamics simulations, Macromol. Theory Simul. 15 (2006) 668–673.
[16] G. Pan, C.W. Manke, Developments toward simulation of entangled polymer melts by dissipative particle dynamics (dpd), Int. J. Mod. Phys. B. 17 (2003) 231–235.
[17] L.L. Xiao, S. Chen, C.S. Lin, Y. Liu, Simulation of a single red blood cell flowing through a microvessel stenosis using dissipative particle dynamics, Mol. Cell. Biomech. MCB. 11 (2014) 67–85.
[18] L.L. Xiao, C.S. Lin, S. Chen, Y. Liu, B.M. Fu, W.W. Yan, Effects of red blood cell aggregation on the blood flow in a symmetrical stenosed microvessel, Biomech. Model. Mechanobiol. (2019).
[19] C. Lin, S. Chen, L. Xiao, Y. Liu, Tuning drop motion by chemical chessboard-patterned surfaces: a many-body dissipative particle dynamics study, Langmuir 34 (2018) 2708–2715.
[20] K. Zhang, S. Chen, Y. Wang, Ratio dependence of contact angle for droplet wetting on chemically heterogeneous substrates, Colloids Surf, Physicochem. Eng. Asp. 539 (2018) 237–242.
[21] P.J. Hoogerbrugge, J.M.V.A. Koelman, Simulating microscopic hydrodynamic phenomena with dissipative particle dynamics, EPL europhys. Lett. 19 (1992) 155.
[22] P. Español, P. Warren, Statistical mechanics of dissipative particle dynamics, EPL europhys. Lett. 30 (1995) 191.
[23] P. Español, M. Serrano, I. Zuñiga, Coarse-graining of a fluid and its relation with dissipative particle dynamics and smoothed particle dynamic, Int. J. Mod. Phys. C 8 (1997) 899–908.
[24] R.D. Groot, P.B. Warren, Dissipative particle dynamics: bridging the gap between atomistic and mesoscopic simulation, J. Chem. Phys. 107 (1997) 4423–4435.
[25] A. Di Renzo, F.P. Di Maio, Comparison of contact-force models for the simulation of collisions in DEM-based granular flow codes, Chem. Eng. Sci. 59 (2004) 525–541.
[26] H.A. Navarro, M.P. De Souza Braun, Determination of the normal spring stiffness coefficient in the linear spring–dashpot contact model of discrete element method, Powder Technol. 246 (2013) 707–722.
[27] A. Ruiz-Angulo, M.L. Hunt, Measurements of the coefficient of restitution for particle collisions with ductile surfaces in a liquid, Granul. Matter 12 (2010) 185–191.
[28] P.A. Moysey, M.R. Thompson, Determining the collision properties of semi-crystalline and amorphous thermoplastics for DEM simulations of solids transport in an extruder, Chem. Eng. Sci. 62 (2007) 3699–3709.
[29] J. Shäfer, S. Dippel, D.E. Wolf, Force schemes in simulations of granular materials, J. Phys. I. 6 (1996) 5–20.
[30] S. Chen, N. Phan-Thien, B.C. Khoo, X.J. Fan, Flow around spheres by dissipative particle dynamics, Phys. Fluids 18 (2006) 1036051994-Present.
[31] L. Yang, H. Yin, Parametric study of particle sedimentation by dissipative particle dynamics simulation, Phys. Rev. E 90 (2014) 033311.
[32] F.L. Chen, X. He, H.M. Yin, Manufacture and multi-physical characterization of aluminum/high-density polyethylene functionally graded materials for green energy building envelope applications, Energy Build. 116 (2016) 307–317.